Kinematic response of single piles for different boundary conditions: analytical solutions and normalization schemes

by

George Anoyatis
Department of Civil Engineering, University of Patras, Rio, Greece

Raffaele Di Laora
Department of Civil Engineering, Second University of Naples, Aversa (CE), Italy

Alessandro Mandolini
Department of Civil Engineering, Second University of Naples, Aversa (CE), Italy

George Mylonakis (Corresponding author)
Department of Civil Engineering,
University of Patras, Rio, Greece, GR-26500
Phone: +30-2610-996542
Fax: +30-2610-996576
e-mail: mylo@upatras.gr

Abstract

Kinematic pile-soil interaction is investigated analytically through a Beam-on-Dynamic-Winkler-Foundation model. A cylindrical vertical pile in a homogeneous stratum, excited by vertically-propagating harmonic shear waves, is examined in the realm of linear viscoelastic material behaviour. New closed-form solutions for bending, as well as displacements and rotations atop the pile, are derived for different boundary conditions at the head (free, fixed) and tip (free, hinged, fixed). Contrary to classical elastodynamic theory where pile response is governed by six dimensionless ratios, in the realm of Winkler analysis three dimensionless parameters suffice for describing pile-soil interaction: (1) a mechanical slenderness accounting for geometry and pile-soil stiffness contrast, (2) a dimensionless frequency (which is different from the classical elastodynamic parameter $a_0 = \omega d / V_s$), (3) soil material damping. With reference to kinematic pile bending, insight into the physics of the problem is gained through a rigorous superposition scheme involving an infinitely-long pile excited kinematically, and a pile of finite length excited by a concentrated force and a moment at the tip. It is shown that for long piles kinematic response is governed by a single dimensionless frequency parameter, leading to a single master curve pertaining to all pile lengths and pile-soil stiffness ratios.

Notation

Latin symbols

a_{cutoff}	cutoff frequency
a_0	dimensionless frequency
a_s	soil acceleration
A_p	pile cross-sectional area
A , B , C , D	integration constants
c	Winkler dashpot coefficient
d	pile diameter
E_p	pile Young's modulus
E_s, G_s	soil Young's modulus, soil shear modulus
H	thickness of soil layer
I_p	pile cross-sectional moment of inertia
I_u	translational kinematic response factor
I_φ, I_θ	rotational kinematic response factors
k^*	complex-valued Winkler modulus
k	dynamic Winkler stiffness
$L\ (=H)$	pile length, soil thickness
M	bending moment
$\tilde{m}_r$	mass per unit pile length
Q	shear force
q	soil wavenumber
CR_z	pile-soil curvature ratio at depth z
CR_0	pile head curvature over soil surface curvature (z=0)
CR_L	pile tip curvature over soil surface curvature (z=L)
u_{ff}	free-field displacement

u_{ff_0} free-field displacement amplitude

u_g base displacement

u_{g_0} base displacement amplitude

V_s^* complex-valued soil shear wave propagation velocity

w pile displacement

z vertical coordinate

$(1/R)_c$ complementary curvature at depth z

$(1/R)_p$ pile curvature at depth z

$(1/R)_{p_0}$ pile curvature at head (level $z=0$)

$(1/R)_{p_0,static}$ static pile curvature at head (level $z=0$)

$(1/R)_s$ soil curvature at depth z

Greek symbols

β Winkler damping coefficient

β_s soil material damping coefficient

Γ dimensionless response coefficient

δ Winkler stiffness coefficient ($=k/E_s$)

λ Winkler wavenumber

λ_{static} static Winkler "wavenumber"

ν_s soil Poisson's ratio

ρ_s, ρ_p soil, pile mass density

τ soil shear stress

ω cyclic excitation frequency

Keywords: pile, kinematic interaction, subgrade reaction, Winkler model, closed-form solution

1 Introduction

It is well known that the passage of seismic waves through soft soil causes deformations in the soil mass that excite dynamically embedded bodies such as piles. As a result, a pile foundation will, even in the absence of a superstructure, be subjected to a spatially-variable displacement field imposed by the surrounding soil which gives rise to a dynamic interplay known as "kinematic interaction" [1, 2, 3]. The ensuing deformations naturally coexist with motions transmitted onto the pile through the pile cap due to structural dynamics, an effect commonly referred to as "inertial interaction" [1, 2, 3]. Note that inertial interaction is affected by kinematic interaction as the input motion to the former problem is the output motion of the latter [4, 5, 6, 7].

Starting with the pioneering work by Blaney et al [8], a large number of analytical studies have demonstrated the importance of kinematic effects on piles [9, 10, 11, 12, 13, 14]. In addition to the theoretical work, post-earthquake investigations [15, 16, 17] have highlighted the vulnerability of pile foundations (even in non-liquefied soil) by revealing damage at the pile head and/or depths where inertial forces are negligible. Seismic regulations [18, 19] have acknowledged the accumulated evidence, enforcing the evaluation of kinematic effects in design of deep foundations, even though only in the presence of a layered profile. Note in this regard that a wealth of research results have demonstrated that significant kinematic bending can develop at the pile head even in perfectly homogeneous soil [12, 20, 21, 22, 23].

The simplest approach for computing kinematic bending along a pile is to neglect pile-soil interaction and assume that pile and soil movement coincides at all times. This procedure has been suggested by Margason [9] and yields the following predictive equation for pile bending moment:

$$M = E_p I_p \left(1/R\right)_p = E_p I_p \left(1/R\right)_s = E_p I_p \frac{a_s}{V_s^2} \quad (1)$$

where E_p and I_p are the Young's modulus and the cross-sectional moment of inertia of the pile, $\left(1/R\right)_p$ and $\left(1/R\right)_s$ are the pile and soil curvature, respectively, $\mathrm{a}_s = \mathrm{a}_s(z,t)$ or $\mathrm{a}_s = \mathrm{a}_s(z,\omega)$ is the depth-varying horizontal ground acceleration and V_s is the shear wave propagation velocity in the soil. A drawback of this approach lies clearly in the inability of Eq. (1) to handle layered soil (as soil curvature is infinite at interfaces separating soil layers of different stiffness) and boundary conditions at the pile head and tip. For instance, Eq. (1) would always predict maximum bending at the pile head even in the absence of a restraining cap (free head conditions).

To account for pile-soil interaction and, thereby, stiffness mismatch between pile and soil as well as different boundary conditions at the ends of the pile, various analytical techniques have been developed over the past decades. A particularly attractive family of methods are the Winkler models which consider the pile as a beam connected to a bed of independent springs and dashpots distributed along its axis, to simulate the restraining and dissipative action of the soil. On the basis of this approach, Flores-Berrones & Whitman [10] derived (implicitly) the ratio of pile and soil curvature for a fixed-head pile embedded in a homogeneous halfspace under harmonic excitation consisting of vertically-propagating S waves. In this case, pile-to-soil curvature ratio was found to be always smaller than unity and to decrease with frequency, thus reflecting the inability of the pile to follow short wavelengths in the soil.

Further studies by Dobry and O'Rourke [11], Mylonakis [13], Nikolaou et al [16] and de Sanctis et al [20], resulted in a number of analytical solutions and empirical

formulas for bending of piles embedded in homogeneous or two-layer soil, showing that pile curvature may exceed soil curvature under certain conditions. Other contributions [17, 24, 25, 26, 27, 28, 29, 30] have investigated the behaviour of piles in two- and multi-layer soil deposits under both harmonic and transient excitation.

Despite these efforts, certain fundamental mechanisms governing the development of bending along kinematically-loaded piles remain poorly understood, even for idealized conditions such as homogeneous soil and low-frequency seismic excitation. Of particular interest are counterintuitive cases where pile curvature is larger than soil curvature and the role of boundary conditions at pile head and tip. The work at hand aims at offering insight into these aspects by: (1) presenting a new set of analytical solutions pertaining to different boundary conditions; (2) introducing new dimensionless parameters governing static and dynamic pile response to vertically-propagating SH waves.

2 Problem definition

The problem considered is depicted in Fig. 1: a single vertical cylindrical pile of length L, diameter d, mass density ρ_p and Young's modulus E_p is embedded in a homogeneous soil layer of thickness $H(=L)$ resting on a rigid base. Soil is modelled as a linear elastic material of Poisson's ratio ν_s, mass density ρ_s and frequency-independent material damping β_s, expressed through a complex-valued shear modulus $G_s^* = G_s(1+2i\beta_s)$. The pile is loaded by vertically propagating shear waves expressed in the form of a harmonic horizontal displacement $u_g(t) = u_{g_0} \exp[i\omega t]$ applied at rock level. Considering different boundary conditions at the pile head

(fixed, free to rotate) and pile tip (fixed, hinged, free to displace and rotate), provides six distinct cases to be examined (Fig. 1). Positive notation for stresses and displacements is provided in Fig. 2.

The problem at hand is governed by seven dimensional parameters (L, d, E_p, E_s, ω, ρ_p, ρ_s), in addition to the inherently dimensionless ratios β_s and ν_s. Given that three fundamental dimensions are involved (Mass, Time, Length), Buckingham's theorem [31] suggests that the interaction problem can be fully described by six $(=7+2-3)$ dimensionless ratios (e.g., L/d, E_p/E_s, ν_s, ρ_p/ρ_s, β_s and $\omega d/V_s$). As will be shown in the ensuing, the adopted Winkler model leads to a drastic reduction in the number of governing independent variables. In particular, response in the static regime is found to be controlled by a unique dimensionless variable, whereas in the dynamic regime two parameters are generally sufficient for describing the interaction problem. It will also be shown that in the realm of the Winkler model, pile-soil interaction for long piles can be described through a single backbone curve, depending solely on a novel frequency parameter.

Solutions from such analyses can be conveniently expressed through the so-called *kinematic response factors I_u and I_φ*. These are defined, respectively, as the translation and rotation amplitudes at the pile head normalized by the corresponding displacement amplitude at the surface of the free-field soil i.e. [8],

$$I_u \equiv \frac{w(0,\omega)}{u_{ff}(0,\omega)} \tag{2}$$

$$I_{\varphi} \equiv \frac{w'(0,\omega)\, d}{u_{ff}(0,\omega)} \tag{3}$$

$w(z,\omega)$ and $u_{ff} = u_{ff}(z,\omega)$ is the frequency- and depth-dependent displacement of the pile and the free-field soil, respectively, and $d =$ pile diameter.

Likewise, the following curvature ratios between pile and soil can be defined as

$$CR_0 = \frac{(1/R)_p\,|_{z=0}}{(1/R)_s\,|_{z=0}} = \frac{w''(0,\omega)\, V_s^2}{a_s(0,\omega)} \tag{4}$$

$$CR_L = \frac{(1/R)_p\,|_{z=L}}{(1/R)_s\,|_{z=0}} = \frac{w''(L,\omega)\, V_s^2}{a_s(0,\omega)} \tag{5}$$

$$CR_z = \frac{(1/R)_p}{(1/R)_s\,|_{z=0}} = \frac{w''(z,\omega)\, V_s^2}{a_s(0,\omega)} \tag{6}$$

corresponding to the pile head (CR_0), pile tip (CR_L) and an arbitrary elevation (CR_z). In the above equations $(\,)''$ denotes double differentiation with respect to depth.

3 Model development

Following earlier studies, the problem is treated in the context of two modular problems, namely the analysis of free-field soil response and the response of the pile. Each sub-problem is addressed separately below.

3.1 **Free-field response**

In one-dimensional analysis, the linear stress-strain law is according to the notation of Fig. 2

$$\tau = -G_s^* \frac{\partial u_{ff}}{\partial z} \tag{7}$$

where G_s^* is the complex soil shear modulus, τ is the shear stress and $u_{ff} = u_{ff}(z,t)$ is the time- and depth-dependent displacement in the free-field soil.

Considering forced harmonic oscillations of the type $u_{ff}(z,t) = u_{ff}(z)e^{i\omega t}$, the equilibrium of forces in the horizontal direction acting upon an arbitrary soil element yields the familiar second-order differential equation

$$\frac{du_{ff}^2}{dz^2} + q^2 u_{ff} = 0 \tag{8}$$

where $V_s^* = V_s\sqrt{1+2i\beta_s}$ and $q = \omega / V_s^*$ is the complex shear wave propagation velocity in the soil and the corresponding wavenumber, respectively.

Solving Eq. (8) and imposing the boundary condition of a traction-free soil surface, the following simple solution is obtained [32]

$$u_{ff}(z,t) = u_{ff_0}\cos(qz)\,e^{i\omega t} \tag{9}$$

which describes a standing wave of amplitude u_{ff_0} at soil surface $(z=0)$. Assuming that the amplitude of motion at base level $(z=H)$ is known, the familiar amplification function is recovered [32, 33]

$$\frac{u_{ff_0}}{u_{g_0}} = \frac{1}{\cos\left(\omega H / V_s^*\right)} \tag{10}$$

3.2 **Pile response**

In the realm of the approach at hand, free-field displacements are applied at the base of the Winkler supports, which constitute the dynamic excitation that forces the pile to deflect. The equilibrium of horizontal forces acting on an arbitrary pile segment yields the governing equation (Fig. 2)

$$\frac{\partial Q}{\partial z} - k^*(w - u_{ff}) - \tilde{\imath}_{r} \frac{\partial^2 w}{\partial t^2} \qquad) \tag{11}$$

where $Q(z,t)$ is shear force, $\tilde{\imath}_{r}$ mass density per unit pile length and $w = w(z,t)$ pile displacement. $k^* = k + i\,\omega c$ is the complex-valued Winkler modulus, k being the stiffness of the Winkler springs and c the corresponding dashpot coefficient [3, 34, 35].

Considering forced harmonic oscillations of the type $w(z,t) = w(z)\exp[i\omega t]$ and given that shear force is related to displacement through the strength-of-materials expression [36]

$$Q(z,t) = -E_p I_p \frac{\partial^3 w}{\partial z^3} \tag{12}$$

the equation governing pile motion can be rewritten in the Navier form [10, 16, 35]

$$\frac{d^4 w}{dz^4} + 4\lambda^4 w = \frac{k^*}{E_p I_p} u_{ff} \tag{13}$$

where $\lambda = \lambda(\omega)$ is the characteristic wavenumber governing the attenuations of pile displacement with depth

$$\lambda = \left(\frac{k + i\omega c - \omega^2 \tilde{r}}{4E_p I_p} \right)^{1/4} \tag{14}$$

Note that even though λ is complex-valued, no superscript ()* is used to distinguish it from real-valued counterparts for the sake of simplicity.

The general solution to the above equation is

$$w(z,\omega) = \left(A\cos\lambda z + B\sin\lambda z\right)e^{-\lambda z} + \left(C\cos\lambda z + D\sin\lambda z\right)e^{\lambda z} + \Gamma\, u_{ff}(z,\omega) \tag{15}$$

where A, B, C, D are integration constants dependent on the boundary conditions; Γ is a dimensionless response coefficient given by [10]

$$\Gamma = \frac{k + i\omega c}{E_p I_p (q^4 + 4\lambda^4)} \tag{16}$$

3.3 **Pile-soil curvature ratio**

Enforcing the boundary conditions at the pile tip, the ratios of pile curvature at the pile head and the corresponding soil curvature at the same elevation, CR_0, for a fixed-head pile are obtained as (Eq. (4)):

$$CR_0 = \Gamma\left[1-2\frac{\begin{array}{r}\cos(qL)\left[\cos(\lambda L)\sinh(\lambda L)+\cosh(\lambda L)\sin(\lambda L)\right]+\\ +\frac{q}{\lambda}\sin(\lambda L)\sinh(\lambda L)\sin(qL)\end{array}}{\sin(2\lambda L)+\sinh(2\lambda L)}\right] \tag{17}$$

$$CR_0 = \Gamma\left[1-2\frac{\cos(qL)\left[\cos(\lambda L)\cosh(\lambda L)-2(1-1/\Gamma)\left(\frac{\lambda}{q}\right)^2\sin(\lambda L)\sinh(\lambda L)\right]}{\cos(2\lambda L)+\cosh(2\lambda L)}\right] \tag{18}$$

$$CR_0 = \Gamma\left[1-2\frac{\begin{array}{r}2(1-1/\Gamma)\left(\frac{\lambda}{q}\right)^2\left[\cos(\lambda L)\sinh(\lambda L)-\cosh(\lambda L)\sin(\lambda L)\right]\cos(qL)+\\ +2\frac{\lambda}{q}\cos(\lambda L)\cosh(\lambda L)\sin(qL)\end{array}}{\sin(2\lambda L)+\sinh(2\lambda L)}\right] \tag{19}$$

corresponding to free-tip, hinged-tip and fixed-tip conditions, respectively. Equation (18) has been reported in Reference [16].

For a fixed-tip pile, pile curvature at pile tip over soil curvature at surface, CR_L, for fixed- and free-head conditions is respectively (Eq. (5)):

$$CR_L = \Gamma \frac{\left[\begin{array}{l} \cos qL \left[\left(\sin 2\lambda L + \sinh 2\lambda L \right) + 2\left(1 - 1/\Gamma\right)\left(\frac{\lambda}{q}\right)^2 \left(\sin 2\lambda L - \sinh 2\lambda L \right) \right] - \\ \qquad - 2\left(\frac{\lambda}{q}\right)\left(\cos 2\lambda L + \cosh 2\lambda L \right) \sin qL \end{array} \right]}{\sin 2\lambda L + \sinh 2\lambda L}$$

(20)

$$CR_L = \Gamma \frac{\left[\begin{array}{l} \cos qL \left[\left(2 + \cos 2\lambda L + \cosh 2\lambda L \right) + 2\left(1 - 1/\Gamma\right)\left(\frac{\lambda}{q}\right)^2 \left(\cos 2\lambda L - \cosh 2\lambda L \right) \right] + \\ \qquad + 2\left(\frac{\lambda}{q}\right)\left(\sin 2\lambda L - \sinh 2\lambda L \right) \sin qL \; - \; 4\cos \lambda L \, \cosh \lambda L \end{array} \right]}{2 + \cos 2\lambda L + \cosh 2\lambda L}$$

(21)

where Γ is given by Eq. (16).

3.4 **Translational kinematic response factor**

For the aforementioned case of a fixed-head pile, corresponding expressions for the kinematic response coefficient I_u in Eq. (2) (ratio of pile head absolute displacement to free-field surface absolute displacement) under free-tip, hinged-tip and fixed-tip conditions are, respectively

$$I_u = \Gamma \left[1 - \left(\frac{q}{\lambda}\right)^2 \frac{\cos(qL)\left[\cosh(\lambda L)\sin(\lambda L) - \cos(\lambda L)\sinh(\lambda L)\right] - \frac{q}{\lambda}\cos(\lambda L)\cosh(\lambda L)\sin(qL)}{\sin(2\lambda L) + \sinh(2\lambda L)} \right]$$

(22)

$$I_u = \Gamma\left[1-\left(\frac{q}{\lambda}\right)^2 \frac{\cos(qL)\left[2(1-1/\Gamma)\left(\frac{\lambda}{q}\right)^2 \cos(\lambda L)\cosh(\lambda L)+\sin(\lambda L)\sinh(\lambda L)\right]}{\cos(2\lambda L)+\cosh(2\lambda L)}\right] \tag{23}$$

$$I_u = \Gamma\left[1-2\frac{\begin{array}{r}\cos(qL)\left[\cos(\lambda L)\sinh(\lambda L)+\cosh(\lambda L)\sin(\lambda L)\right](1-1/\Gamma)+\\ +\frac{q}{\lambda}\sin(\lambda L)\sinh(\lambda L)\sin(qL)\end{array}}{\sin(2\lambda L)+\sinh(2\lambda L)}\right] \tag{24}$$

Note that for the limit case of an infinitely-long pile, all the above relations converge to the simple solution of Flores-Berrones & Whitman [10]

$$I_u = \Gamma \tag{25}$$

a result which is also valid for curvature ratios. Note that Eq. (22) has been derived (yet inadvertently referred to as curvature ratio CR_0) in Reference [16].

With reference to free-head piles, kinematic response coefficients for free-tip, hinged-tip and fixed-tip conditions are, respectively

$$I_u = \Gamma\left[1+\left(\frac{q}{\lambda}\right)^3 \frac{\sin(qL)\left[\cos(\lambda L)\sinh(\lambda L)-\cosh(\lambda L)\sin(\lambda L)\right]-2\frac{\lambda}{q}\sin(\lambda L)\sinh(\lambda L)\cos(qL)}{\cos(2\lambda L)+\cosh(2\lambda L)-2}\right] \tag{26}$$

$$I_u = \Gamma\left[1+\left(\frac{q}{\lambda}\right)^2 \frac{\begin{array}{r} 2(1-1/\Gamma)\left(\frac{\lambda}{q}\right)^2\left[\cos(\lambda L)\sinh(\lambda L)-\cosh(\lambda L)\sin(\lambda L)\right]\cos(qL)+ \\ +\sin(\lambda L)\left[\cosh(\lambda L)\cos(qL)-\cos(\lambda L)\right]+ \\ +\sinh(\lambda L)\left[\cos(\lambda L)\cos(qL)-\cosh(\lambda L)\right] \end{array}}{\sin(2\lambda L)-\sinh(2\lambda L)}\right] \tag{27}$$

$$I_u = \Gamma\left[1+\left(\frac{q}{\lambda}\right)^2 \frac{\begin{array}{r} -4(1-1/\Gamma)\left(\frac{\lambda}{q}\right)^2\cos(\lambda L)\cosh(\lambda L)\cos(qL)+\left[\cosh(2\lambda L)-\cos(2\lambda L)\right]/2- \\ -2\left(\frac{\lambda}{q}\right)\sin(qL)\left[\cos(\lambda L)\sinh(\lambda L)+\cosh(\lambda L)\sin(\lambda L)\right] \end{array}}{\cos(2\lambda L)+\cosh(2\lambda L)+2}\right] \tag{28}$$

3.5 **Rotational kinematic response factor**

To quantify pile head rotation, a second interaction coefficient can be defined as

$$I_\theta = \frac{w'(0,\omega)}{\lambda\, u_{ff_0}} \tag{29}$$

It should be noticed that the above definition is different from the ordinary coefficient I_φ (note the different subscript) in Eq. (3) invariably employed in the literature [4, 6, 16], as in this way pile head rotation depends solely on dimensionless frequency and Winkler parameter ($\omega / \lambda V_s$) and λL, respectively.

Expressions for I_θ pertaining, respectively, to free-tip, hinged-tip and fixed-tip conditions are:

$$I_\theta = \Gamma\left(\frac{q}{\lambda}\right)^2 \frac{\left[\begin{array}{r} 2\cos(qL)\left[\cosh(\lambda L)\sin(\lambda L)+\cos(\lambda L)\sinh(\lambda L)\right]-\sin(2\lambda L)-\sinh(2\lambda L)+ \\ +2\frac{q}{\lambda}\sin(\lambda L)\sinh(\lambda L)\sin(qL) \end{array}\right]}{\cos(2\lambda L)+\cosh(2\lambda L)-2} \tag{30}$$

$$I_\theta = \Gamma\left(\frac{q}{\lambda}\right)^2 \frac{\left[\begin{array}{r} 2\cos(qL)\left[2(1-1/\Gamma)\left(\frac{\lambda}{q}\right)^2\sin(\lambda L)\sinh(\lambda L)-\cos(\lambda L)\cosh(\lambda L)\right]+ \\ +\cos(2\lambda L)+\cosh(2\lambda L) \end{array}\right]}{\sin(2\lambda L)-\sinh(2\lambda L)} \tag{31}$$

$$I_\theta = \Gamma\left(\frac{q}{\lambda}\right)^2 \frac{\left[\begin{array}{r} 4(1-1/\Gamma)\left(\frac{\lambda}{q}\right)^2\left[\cos(\lambda L)\sinh(\lambda L)-\cosh(\lambda L)\sin(\lambda L)\right]\cos(qL)- \\ -\sin(2\lambda L)-\sinh(2\lambda L)+4\frac{\lambda}{q}\cos(\lambda L)\cosh(\lambda L)\sin(qL) \end{array}\right]}{\cos(2\lambda L)+\cosh(2\lambda L)+2} \tag{32}$$

Discussion of the above analytical developments is provided in the remainder of the article.

4 Interpretation of results & comparison with other solutions

For comparison purposes, rigorous Finite Element (FE) analyses were performed by means of the commercial computer platform ANSYS [37]. Given that the geometry is axisymmetric and the load anti-symmetric, stresses and displacements were expanded in Fourier series along the circumferential direction, following the technique introduced by Wilson [38] and later employed by Blaney et al. [8] and Syngros [39].

For the problem at hand, only the first term of the series is relevant and, thereby, solving a single FE configuration is sufficient. Owing to this procedure, the original three-dimensional problem is conveniently reduced to a two dimensional. The domain was discretised using 4-noded axisymmetric elements; following a sensitivity analysis, the lateral dimension of the model was set equal to 200*d*, to ensure that soil response close to the boundaries is not affected by outward-spreading waves emitted from the pile-soil interface. Likewise, vertical displacements were restrained along the lateral boundary of the mesh to simulate 1-dimensional conditions for S-waves at large distances from the pile. In addition, nodes at the base of the model were fully restrained to represent the rigid bedrock. Vertical size of the elements was kept constant, equal to $d/4$ which was found to be sufficiently accurate and economical. The analyses were carried out in the frequency domain [8, 21, 37], the load being applied in the form of a harmonic horizontal body force in each element.

4.1 **Static Response**

It is well-known that in Winkler models pile-soil interaction is controlled by the key dimensionless parameter [10, 35]

$$\lambda L = L\left(\frac{k}{4E_p I_p}\right)^{1/4} = \left(\frac{16\,\delta}{\pi}\right)^{1/4}\left(\frac{L}{d}\right)\left(\frac{E_p}{E_s}\right)^{-1/4} \tag{33}$$

being the product of λ (evaluated for $\omega = 0$) in Eq. (14) and pile length L. In such models λL is a unique parameter controlling static response, which can be interpreted as a "mechanical slenderness" (as opposed to the familiar geometrical slenderness L/d) as it encompasses both geometry (L/d) and pile-soil relative stiffness (E_p/E_s). In addition, λL is function of the Winkler stiffness coefficient $\delta = k/E_s$, the value of

which lies in the core of the Winkler representation. The effect of δ on kinematic response is examined in Figs. 3 and 4, where pile-soil curvature ratio is plotted against pile slenderness L/d for two values of pile-soil stiffness contrast. It is evident by inspecting Figs. 3 and 4, that the predictions of Winkler models employing the commonly used value $\delta = 1.2$ pertaining to inertial interaction analyses [40, 41], are not in good agreement with the FE results for certain cases examined. In Figs. 3a and 3b the value of δ that matches the FE results seems to decrease with increasing pile slenderness and with decreasing pile-soil stiffness ratio. Moreover, different values for "optimum" δ are obtained depending on boundary conditions at the tip as shown in Figs. 3c and 3d. In addition, optimum δ clearly depends on the parameter to be matched. For instance, it is evident from Figs. 4a and 4b that values of δ matching CR_L (ratio of pile curvature at tip over soil curvature at soil surface) differ from those in Fig. 3, referring to CR_0, and are independent of pile slenderness L/d. In light of this observation, results for static pile-soil curvature ratio presented in Figs. 5 to 14 are plotted in terms of λL.

In Fig. 5, static pile-soil curvature ratio at the pile head is plotted against λL for different boundary conditions at the pile tip. Naturally, all curves start from zero since for $\lambda L \to 0$ the pile degenerates into a rigid disk, thus experiencing zero moment regardless of restraints at the tip. With increasing λL curvature ratio gradually increases attaining unity at points $A_{1,2}$ and A_3, and reaching a maximum, above unity, at points M_1, M_2, M_3 depending on the conditions at the tip. A further increase in λL causes pile curvature to drop and gradually converge to soil curvature ($B_{1,2}$, B_3, T), as the pile becomes sufficiently flexible to follow soil deformation, regardless of tip conditions.

A better understanding of the above trends, which may explain the counterintuitive values of curvature ratios larger than one, may be achieved through a simple mechanistic approach, which interprets the curvature of a fixed-head pile of length L as the superposition of: (1) the curvature of an infinitely-long pile ($CR = 1$ at any depth) and (2) a "complementary" curvature profile accounting for finite pile length and the specific boundary condition at the tip. As an example, for a fixed-head pile the expression for static pile-soil curvature ratio at any depth can be cast in the form:

$$\frac{(1/R)_p}{(1/R)_s} = 1 - \frac{(1/R)_c}{(1/R)_s} \tag{34}$$

where 1 in the right side is the curvature ratio for an infinitely-long fixed-head pile in static regime [for which $(1/R)_p = (1/R)_s$], and $(1/R)_c$ is a "complementary" curvature at depth z as defined above. This interpretation is schematically shown in Fig. 6 for the case of a floating pile (free-tip condition): an infinitely-long pile embedded in homogeneous soil is conceptually separated from the underlain material at depth $z = L$ (Fig. 6a). The curvature pattern of the upper part of the pile in Fig. 6a is tantamount to the superposition of the curvature along a free-tip pile of length L (Fig. 6b) and the complementary curvature of the same pile subjected at its tip to an action $E_p I_p (1/R)_s$ (Fig. 6c), due to the "detached" lower part in Fig. 6a. For this particular case, substituting the expression for $(1/R)_c$ (see [42]), Eq. (34) duly reduces to Eq. (17) for $z = 0$.

The above procedure can be extended to account for the more general case of a restrained pile tip. This can be achieved by introducing in Fig. 6b the pertinent restraining actions at the tip. To ensure equilibrium, the opposite actions must be

applied at pile tip in Fig. 6c. For hinged-tip condition a horizontal force must be applied at the tip, whereas for a fixed-tip both a force and a moment are required. Note that because of the statically indeterminate nature of the problem in Fig. 6b, the values of these restraining actions are not known a priori.

An alternative interpretation of the trends observed in Fig. 5 is possible by means of the aforementioned superposition approach. Indeed, the complementary curvature at the pile head may possess different signs depending on the value of λL. Specifically: for a very short pile the complementary moment at the pile head will be equal to soil curvature, thus leading to a zero overall moment at the top. On the other hand, for an infinitely-long pile curvature at the head will be equal to soil curvature, as the external moment in Fig. 6c will not be transmitted to the pile top. For short piles the moment transmitted to the head has the same sign as the applied moment. This results in pile-soil curvature ratios lower than unity. For longer piles, the complementary moment becomes negative leading to a curvature ratio higher than unity.

The profile of pile curvature with depth over soil curvature at surface, CR_z, is presented in Figs. 7 to 9 for various head and tip conditions and the values of λL shown at the insert of Fig. 5. For fixed-head, free-tip conditions (Fig. 7a) the bending moment along a short pile ($\lambda L <$ 5.49, Fig. 5) attains its maximum value at the top, decreasing monotonically with depth. For long piles ($\lambda L >$ 5.49, Fig. 5) the maximum curvature ratio develops at depth and attains the value of 1.04. The depth $z_{\max}$ corresponding to maximum curvature ratio may be related to λL by means of the aforementioned superposition scheme through the easy-to-derive expressions valid for free-tip conditions

$$\lambda z_{\max} = \lambda L - 3.14, \quad \lambda L > 5.49 \tag{35}$$

For free-head, free-tip piles (Fig. 7b) all curves are symmetrical. Specifically, for $0 < \lambda L < 2\pi$ (short piles) pile bending attains its peak value at mid-depth. For $\lambda L > 2\pi$ (long piles) a maximum is observed at two symmetric distances $\lambda z_{\max} = \pi$ from the head and tip.

Pile-soil curvature ratio for hinged-tip piles is presented in Fig. 8. The behaviour of fixed-head piles depicted in Fig. 8a is similar to the one shown in Fig 7a: bending moment attains its maximum at the top for short piles ($\lambda L <$ 4.71, Fig. 5), whereas for long piles ($\lambda L > 4.71$, Fig. 5) maximum curvature ratio develops at depth and attains a constant value of 1.07. In the same fashion, depth $z_{\max}$ corresponding to the maximum curvature ratio is related to λL through the expression

$$\lambda z_{\max} = \lambda L - 2.4, \quad \lambda L > 4.71 \tag{36}$$

The hinged-tip pile in Fig. 8b experiences a curvature pattern analogous to that in Fig. 7b. The maximum value of curvature ratio is observed at $z = 0.58L$ for $0 < \lambda L < 5.49$ (short piles), whereas for higher values of λL the maximum is observed at the depth given by Eq. (36)

For fixed-tip piles, the maximum curvature is always observed at the tip and has an opposite sign compared to the one at the top (Fig. 9). It is noted in passing that a quick estimate of the curvature ratio at the pile base can be obtained using the expression of Dobry & O'Rourke [11] derived for an infinitely-long pile in two-layer soil,

considering an infinitely-stiff bottom layer. This leads to an overestimation of curvature ratio at the pile tip equal to $2\lambda L$.

4.2 **Dynamic Response**

Employing the approximate relations for the distributed dashpot coefficient along the pile $c = 6a_0^{-1/4}\rho_s V_s d + 2\beta_s \delta E_s / \omega$ derived using planar wave-propagation analysis [34], the complex-valued wavenumber λ can be related to its static value through

$$\frac{\lambda}{\lambda_{static}} = \begin{cases} \left[1 - \dfrac{\pi}{8(1+\nu_s)} \dfrac{\mathrm{a}_0^2}{\delta} \dfrac{\rho_p}{\rho_s} + i\,2\beta_s\right]^{1/4}, & \mathrm{a}_0 \le \mathrm{a}_{cutoff} \\ \left[1 - \dfrac{\pi}{8(1+\nu_s)} \dfrac{\mathrm{a}_0^2}{\delta} \dfrac{\rho_p}{\rho_s} + i\left(\dfrac{3\mathrm{a}_0^{3/4}}{1+\nu_s} \dfrac{1}{\delta} + 2\beta_s\right)\right]^{1/4}, & \mathrm{a}_0 > \mathrm{a}_{cutoff} \end{cases} \tag{37}$$

where λ and λ_{static} are obtained from Eqs. (14) and (33), respectively, and a_{cutoff} stands for a characteristic frequency (termed "cutoff frequency") below which no stress waves can be emitted from the pile-soil interface to propagate horizontally in the soil medium and, thereby, no radiation damping is generated. The cutoff frequency is, therefore, associated with a sudden increase in damping and coincides with the fundamental frequency of the soil layer in shearing and is expressed in dimensionless form as

$$\mathrm{a}_{cutoff} = (\pi / 2)\,(H / d)^{-1} \tag{38}$$

Note that for the range of frequencies relevant to earthquake engineering, the term related to pile density in Eq. (37) may be neglected without significant error.

In the same spirit as in static analysis, dynamic pile response can be described by a unique dimensionless parameter. This is achieved by using the static value of λ in Eq. (33) in the dynamic regime. The validity of the approximation is explored in Fig. 10, in which pile-soil curvature ratio at the head is plotted against frequency $a_0 = \omega d / V_s$ for selected pile-soil configurations. Predictions using the static value of λ in Eq. (33) are compared to those obtained from the complete formulation in Eq. (37) and to FE results. Different values for δ are used for each case, based on an optimal selection according to Fig. 3. A convergence of all curves below cutoff frequency is observed. Beyond cutoff, however, the static assumption leads to a better agreement with the more rigorous FE results. This is probably due to the approximate description of radiation damping employed in Eq. (37) which was based on inertial interaction considerations [34]. Nevertheless, even under a more realistic representation of geometric energy dissipation, the benefit stemming from the simplified approach cannot be overstated. It is also worth noting that optimum δ exhibits only a weak dependence on frequency. Accordingly, optimum δ for static analysis (Fig. 3) can be employed in the dynamic regime (Fig. 10).

Additional comparisons of the proposed model against FE results obtained as part of this study [37] and from the literature [6] are presented in Figs. 11 and 12 in terms of translational and rotational kinematic response factors I_u and I_ϕ. It is evident that the predictions of the model are in satisfactory agreement with the results of the more rigorous solutions for all configurations examined.

In the remainder of the article, dynamic effects are discussed in terms of pile curvature and kinematic response factors I_u and I_θ. In light of the analytical developments in Eqs. (22)-(32), it can be readily recognized that the adoption of a_0

(which is independent of mechanical slenderness) as an independent frequency variable would not allow (λL) to be the main parameter controlling the response. It is observed that the excitation frequency appears in the solutions only in dimensionless terms $qH\ (=\omega H/V_s)$ and $q/\lambda\ (=\omega/\lambda V_s)$, thereby, these frequency parameters can be used for expressing results in the dynamic regime.

For an infinitely-long fixed-head pile, pile-soil curvature ratio at all depths, CR, and kinematic response factor I_u can be cast in the form

$$CR = I_u = \left[1+\frac{1}{4}\left(\frac{\omega}{\lambda V_s^*}\right)^4\right]^{-1} \tag{39}$$

Which coincides with factor Γ in Eq. (16) and clearly indicates that the response of long piles depends solely on the unique frequency parameter $(\omega/\lambda V_s)$ and soil material damping β_s, not on dimensionless frequency a_0.

In Fig. 13, the dynamic de-amplification of curvature ratio at the pile head is plotted against $(\omega/\lambda V_s)$ for fixed-head piles under different boundary conditions at the tip. Dynamic pile curvature decreases with frequency for all piles of finite length, as the pile is unable to follow short wavelengths in the soil. For the trivial case $\lambda L = 0$ dynamic de-amplification is equal to one, as dynamic pile curvature is always zero. With increasing λL all curves approach the one corresponding to the infinitely-long pile regardless of tip conditions. The threshold value of λL beyond which a pile behaves as an infinitely-long beam depends on end condition and is strictly related to the static behaviour depicted in Fig. 5. Indeed, if a pile behaves as an infinitely-long beam under static conditions

($\lambda L >$ 4.71, 5.49 - Fig. 5), it behaves the same way in the dynamic regime. Note that with increasing λL the curves do not evolve in a monotonic manner. Interestingly, the lower curve corresponds to the value of λL for which the curvature ratio is maximum in static conditions (λL corresponding to 2.57, 2.31, π - Fig. 5).

Similar observations can be made for the kinematic response factor I_u (Fig. 14), except for that the threshold values of mechanical slenderness are lower than in the previous case. This pattern may reflect that strains are more sensitive to boundary conditions than displacements.

For free-head piles kinematic response factors I_u and I_θ are plotted in Figs. 15 and 16. A common trend is observed: both factors increase with increasing frequency up to a certain value of $\left(\omega / \lambda V_s\right)$. Beyond this value the trend is reversed with I_u and I_θ decreasing with frequency. This behaviour can be explained in light of wavelengths developing in the soil at different frequencies. With increasing frequency, wavelengths become shorter forcing the pile to experience stronger rotations along its length. This also leads to higher displacements atop free-head piles. Note that the maximum rotation at the pile head is equal to the ratio of free-field displacement

at the soil surface, u_{ff_0}, and the characteristic wavelength of the pile, $\left(1/\lambda\right)$.

5 CONCLUSIONS

A Beam-on-Dynamic-Winkler-Foundation model was employed to investigate the behaviour of kinematically stressed piles of finite length embedded in a homogeneous

soil layer, for different boundary conditions at the head and tip. Analytical solutions for pile response were provided in closed form.

The main conclusions of the study may be summarized as follows:

1) Owing to its simplicity, the adopted analytical model can shed light on certain fundamental mechanisms controlling pile-soil interaction. Its performance, however, is related to a proper selection of stiffness coefficient δ which depends on a number of parameters such as pile slenderness, pile-soil stiffness ratio, boundary conditions, as well as on the parameter to be matched (i.e., pile curvature, pile displacement, etc). Nevertheless, it is observed (Fig. 3) that δ attains higher values for small pile slenderness and large pile-soil stiffness ratios, and appears to be independent of frequency (Figs. 3 and 10).

2) In Winkler models, pile-soil kinematic interaction is governed by a unique dimensionless parameter, λL, (Eq. (33)) which can be interpreted as a "mechanical slenderness", encompassing key problem parameters namely pile slenderness, pile-soil stiffness ratio and Winkler coefficient δ. A unique parameter (λL) governs the response at static conditions. The same parameter controls the behaviour in the dynamic regime if pile inertia and radiation damping are neglected. This simplification allows for a better understanding of the interaction phenomenon and leads to a better agreement of the closed-form solutions with rigorous numerical results.

3) Pile curvature may be decomposed into the sum of soil curvature and a complementary curvature that develops along the pile subjected to pertinent forces and moments at the two ends. These forces depend on the specific boundary

conditions and are responsible for the counterintuitive phenomenon of pile curvature higher than soil curvature for certain values of pile slenderness.

4) A new dimensionless frequency factor $\left(\omega / \lambda V_s\right)$ was introduced for normalizing response in the dynamic regime. It was shown that this allows long piles to exhibit the same response regardless of actual length and pile-soil stiffness ratio. This can be understood, since the dimensionless frequency is expressed as ratio of characteristic pile wavelength $\left(1/\lambda\right)$ and soil wavelength $\left(V_s/\omega\right)$ at a given frequency. As a follow up, a new kinematic response factor was introduced to describe pile head rotation (Eq. (29)). In this way, the interaction is function only of the aforementioned frequency factor and mechanical slenderness.

Acknowledgements

The research reported in this paper was conducted under the auspices of the ReLUIS project "Methods for risk evaluation and management of existing buildings", funded by the Italian National Emergency Management Agency and was partially supported by the University of Patras through a Caratheodory Grant (No. C.580). The authors are grateful for this support. The authors also would like to thank the anonymous Reviewers whose comments improved the quality of the manuscript.

References

[1] Roesset JM, Whitman RV, Dobry R. Modal analysis for structures with foundation interaction. Journal of the Structural Division 1973; 99 (3): 399-416.

[2] Wolf JP. Dynamic Soil–Structure Interaction. Englewood Cliffs, NJ, Prentice-Hall, 1985.

[3] Gazetas G, Mylonakis G. Seismic soil-structure interaction: new evidence and emerging issues, in Geotechnical Earthquake Engineering and Soil Dynamics III ASCE, eds. P. Dakoulas, Evl. K. Yegian, and R. D. Holtz, 1998

[4] Kaynia AM, Kausel E. Dynamic stiffness and seismic response of pile groups. Research Report R82-03. Cambridge, MA: Massachusetts Institute of Technology, 1982.

[5] Mamoon SM, Banerjee PK. Response of piles and pile groups to travelling SH waves. Earthquake Engineering and Structural Dynamics 1990; 19:597-610.

[6] Fan K, Gazetas G, Kaynia A, Kausel E, Ahmad S. Kinematic seismic response of single piles and piles groups. Journal of Geotechnical Engineering Division ASCE 1991; 117(12):1860-1879.

[7] Rovithis E, Mylonakis G, Pitilakis K. Inertial and kinematic response of piles in layered inhomogeneous soil: Winkler analysis. Second International Conference on Performance-Based Design in Earthquake Geotechnical Engineering, 28-30 May, Taormina, ID:11.21, 2012.

[8] Blaney GW, Kausel E, Roesset JM. Dynamic stiffness of piles, in Proceedings in 2nd International Conference on Numerical Methods in Geomechanics ASCE, Blackburg, Virginia, 1976.

[9] Margason E. Pile bending during earthquakes. Lecture ASCE/UC-Berkeley seminar on design construction & performance of deep foundations, 1975.

[10] Flores-Berrones R, Whitman RV. Seismic response of end-bearing piles.Journal of Geotechnical Engineering Division ASCE 1982; 108(4):554-569.

[11] Dobry R, O'Rourke MJ. Discussion on "Seismic response of end-bearing piles" by Flores-Berrones R & Whitman RV," Journal of the Geotechnical Engineering Division 1983, p. 109.

[12] Kavvadas M, Gazetas G. Kinematic seismic response and bending of free-head piles in layered soil. Géotechnique 1993; 43(2):207-222.

[13] Mylonakis G. Analytical solutions for seismic pile bending. Unpublished research report, City University of New York, 1999.

[14] Mylonakis G. Simplified model for seismic pile bending at soil layer interfaces. Soils and Foundations 2001; 41(4):47-58.

[15] Tazoh T, Shimizu K, Wakahara T. Seismic observations and analysis of grouped piles. Dynamic response of pile foundations: experiment, analysis and observation. Geotechnical Special Publication 1987; 11:1-20.

[16] Nikolaou AS, Mylonakis G, Gazetas G, Tazoh T. Kinematic pile bending during earthquakes analysis and field measurements. Géotechnique 2011: 51(5):425-440.

[17] Di Laora R, Mandolini A, Mylonakis G. Insight on kinematic bending of flexible piles in layered soil. Soil Dynamics and Earthquake Engineering 2012, 43:309-322.

[18] CEN/TC 250. Eurocode 8. Design of structures for earthquake resistance Part 5: Foundations, retaining structures and geotechnical aspects. European Committee for Standardization Technical Committee 250, Standard EN 1998–5, Brussels, Belgium, 2003.

[19] National Earthquake Hazard Reduction Program. Recommended provisions for the development of seismic regulations for new buildings. FEMA publication 274, Building Seismic Safety Council, Washington, D.C., 1997.

[20] de Sanctis L, Maiorano RMS, Aversa S. A method for assessing kinematic bending moments at the pile head. Earthquake Engineering and Structural Dynamics 2010; 39:375–397.

[21] Di Laora R. Seismic soil-structure interaction for pile supported systems. Ph.D. Thesis, University of Napoli "Federico II", Napoli, 2009.

[22] Di Laora R, Mylonakis G, Mandolini A. Pile-head kinematic bending in layered soil. Earthquake Engineering and Structural Dynamics 2012; DOI: 10.1002/eqe.2201.

[23] Di Laora R, Mandolini A, Mylonakis G. Selection criteria for pile diameter in seismic areas. Second International conference on Performance-based Design in Earthquake Geotechnical Engineering. 28-30 May, Taormina, Italy. ID:10.15, 2012.

[24] Pender M. Seismic pile foundation design analysis. Bulletin of the New Zealand National Society for Earthquake Engineering 1993; 26(1):49-160.

[25] Kaynia AM, Mahzooni S. Forces in pile foundations under seismic loading. Journal of Engineering Mechanics ASCE 1996; 122(1):46-53.

[26] Castelli F, Maugeri M. Simplified approach for the seismic response of a pile foundation. Journal of Geotechnical and Geoenvironmental Engineering 2009; 135(10):1440-1451.

[27] Maiorano RMS, de Sanctis L, Aversa S, Mandolini A. Kinematic response analysis of piled foundations under seismic excitations. Canadian Geotechnical Journal 2009; 46(5):571-584.

[28] Dezi F, Carbonari S, Leoni G. Kinematic bending moments in pile foundations. Soil Dynamics and Earthquake Engineering 2009; 30(3):119-132.

[29] Sica S, Mylonakis G, Simonelli AL. Transient kinematic pile bending in two-layer soil. Soil Dynamics and Earthquake Engineering 2011; 31(7): 891-905.

[30] Cairo R, Chidichimo A. Nonlinear analysis for pile kinematic response. Fifth International Conference on Earthquake Geotechnical Engineering. Santiago (Chile), 10-13 January, 2011.

[31] Buckingham E. On physically similar systems; illustrations of the use of dimensional equations. Physical Review 1914; 4(4):345-376.

[32] Kramer SL. Geotechnical Earthquake Engineering. New York: Prentice-Hall, 1996.

[33] Roesset JM. Soil amplification of earthquakes, in Numerical Methods in Geotechnical Engineering (Eds. Desai CS and Christian JT), New York, McGraw-Hill, 1977.

[34] Gazetas G, Dobry R, Horizontal response of piles in layered soils. Journal of Geotechnical Engineering ASCE 1984; 110(1): 20-40.

[35] Mylonakis G. Contributions to Static and Dynamic Analysis of Piles and Pile-Supported Bridge Piers. Ph.D. Thesis, State University of New York at Buffalo, 1995.

[36] Den Hartog JP. Advanced Strength of Materials. New York: McGraw-Hill, 1952.

[37] Inc., ANSYS. ANSYS Theory Reference 10.0. Canonsburg, Pennsylvania, US, 2005.

[38] Wilson EL. Structural analysis of axisymmetric solids. American Institute of Aeronautics and Astronautics Journal AIAA 1965; 3:2269-2274.

[39] Syngros C. Seismic response of piles and pile-supported bridge piers evaluated through case histories. Ph.D. Thesis , City University of New York, 2004.

[40] Novak M, Nogami T, Aboul-Ella F. Dynamic soil reactions for plane strain case. Journal of the Engineering Mechanics Division ASCE 1978; 104(4):953-959.

[41] Roesset JM. The use of simple models in soil-structure interaction, in ASCE specialty conference, Civil Engineering and Nuclear Power, Knoxville, TN, 1980.

[42] Hetenyi M. Beams on Elastic Foundations. Michigan: University of Michigan Press, Ann Arbor, 1946.

FIGURES

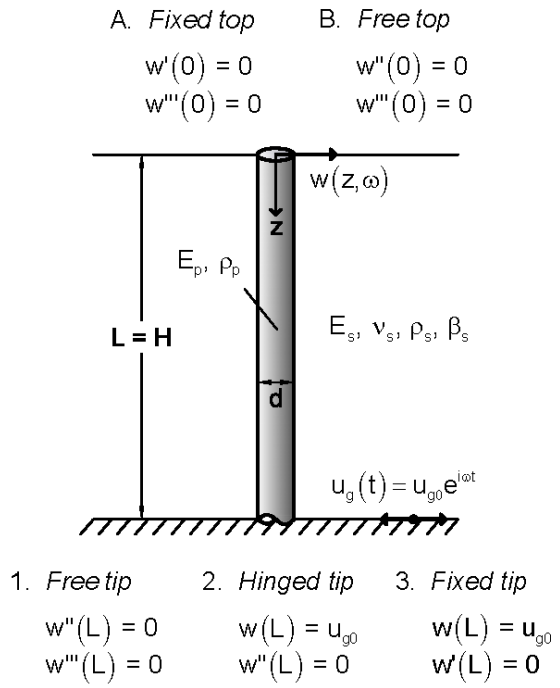

Fig. 1. Problem considered and associated boundary conditions at pile head and tip.

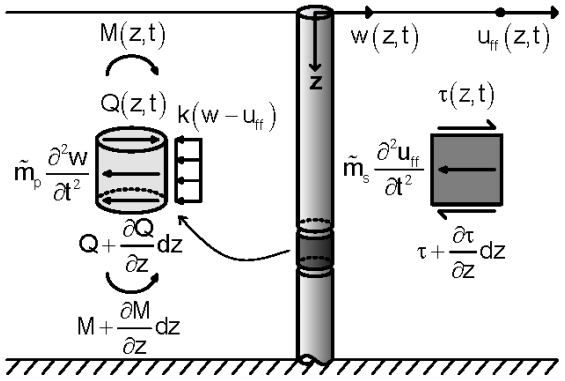

Fig. 2. Positive notation for forces and stresses on pile and soil, respectively.

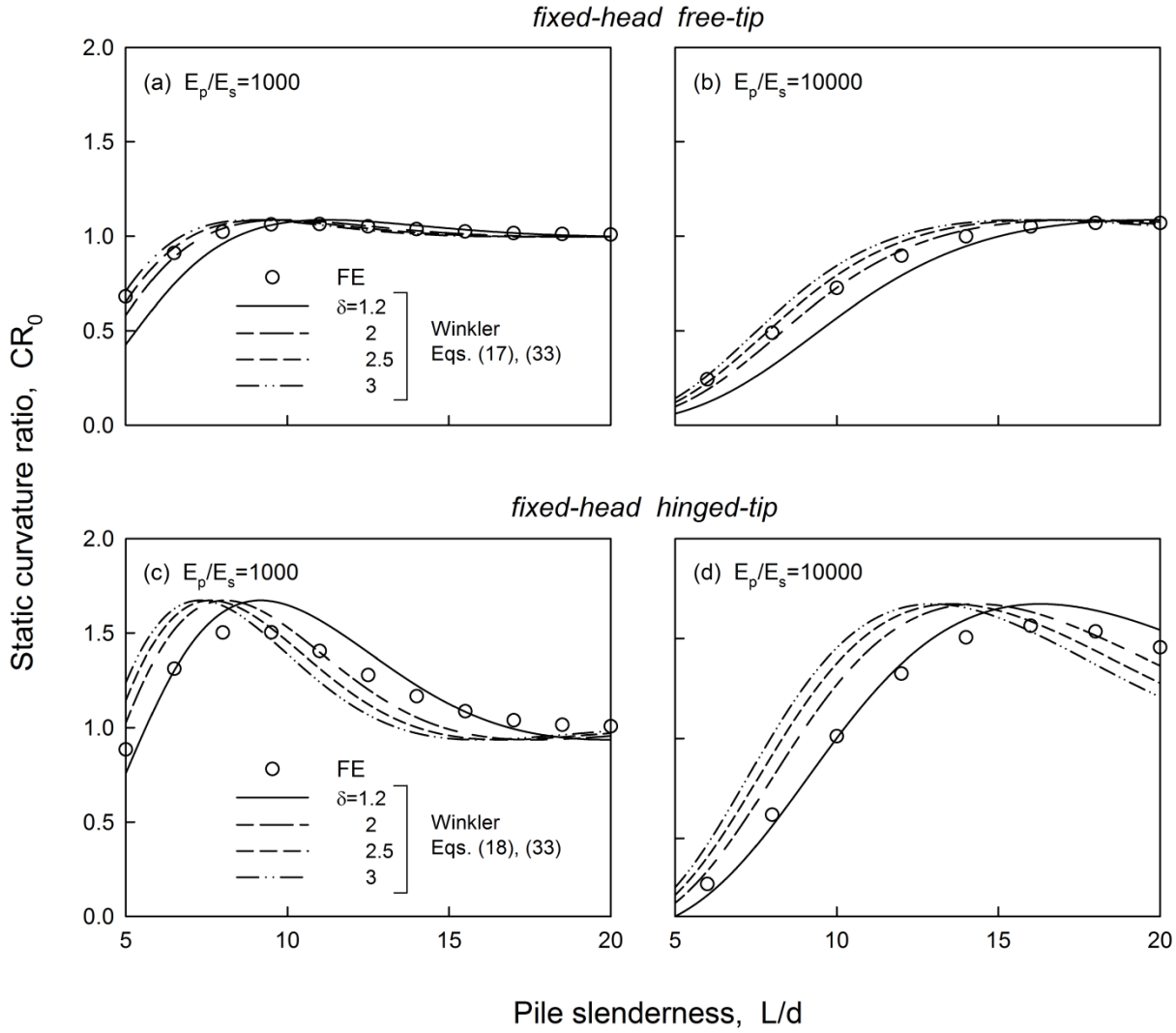

Fig. 3. Variation of pile-soil curvature ratio at pile head under static conditions (ω=0), as function of pile slenderness for selected values of Winkler stiffness parameter δ.

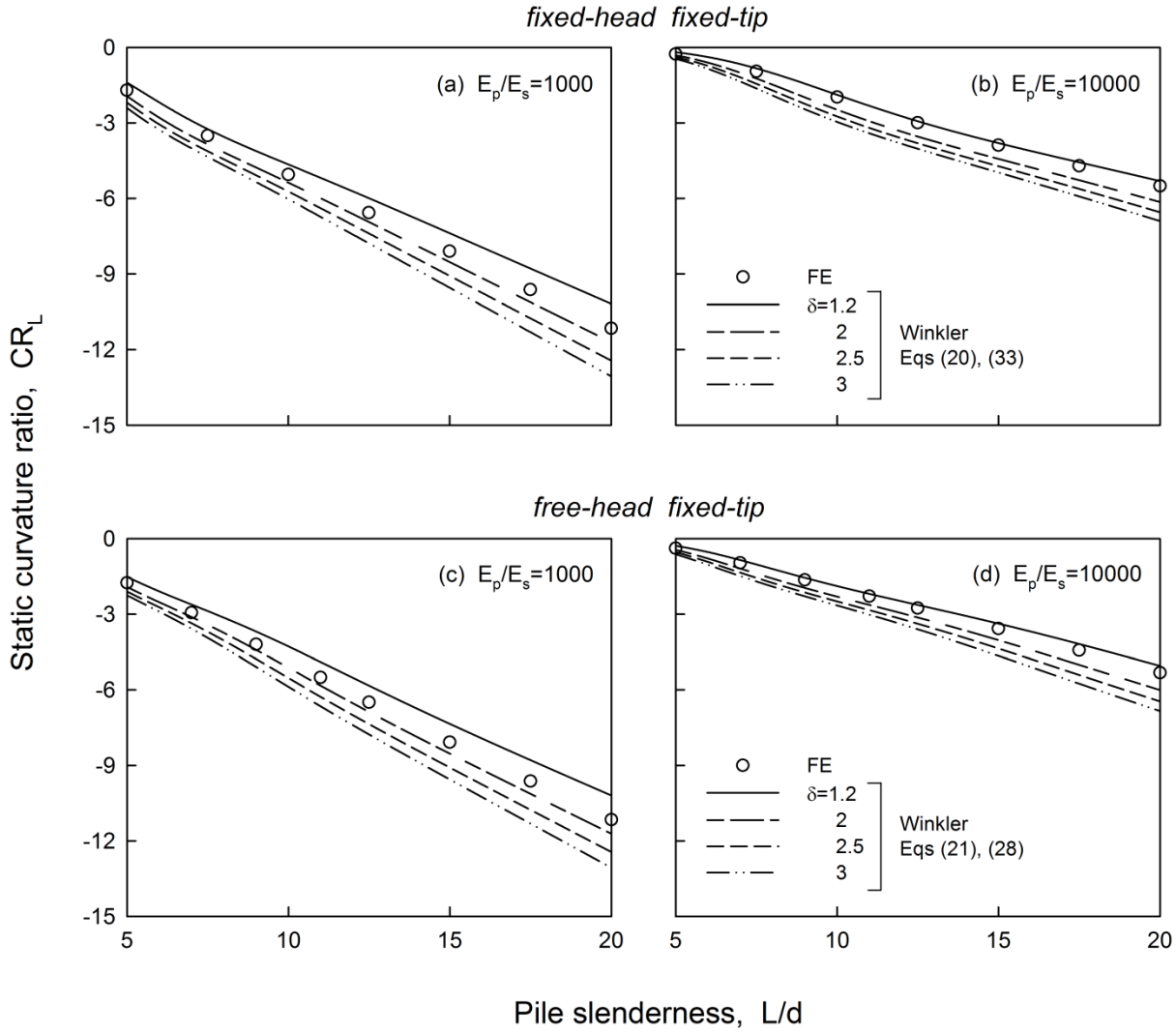

Fig. 4. Variation of pile-soil curvature ratio at pile tip under static conditions (ω=0), as function of pile slenderness for selected values of Winkler stiffness parameter δ.

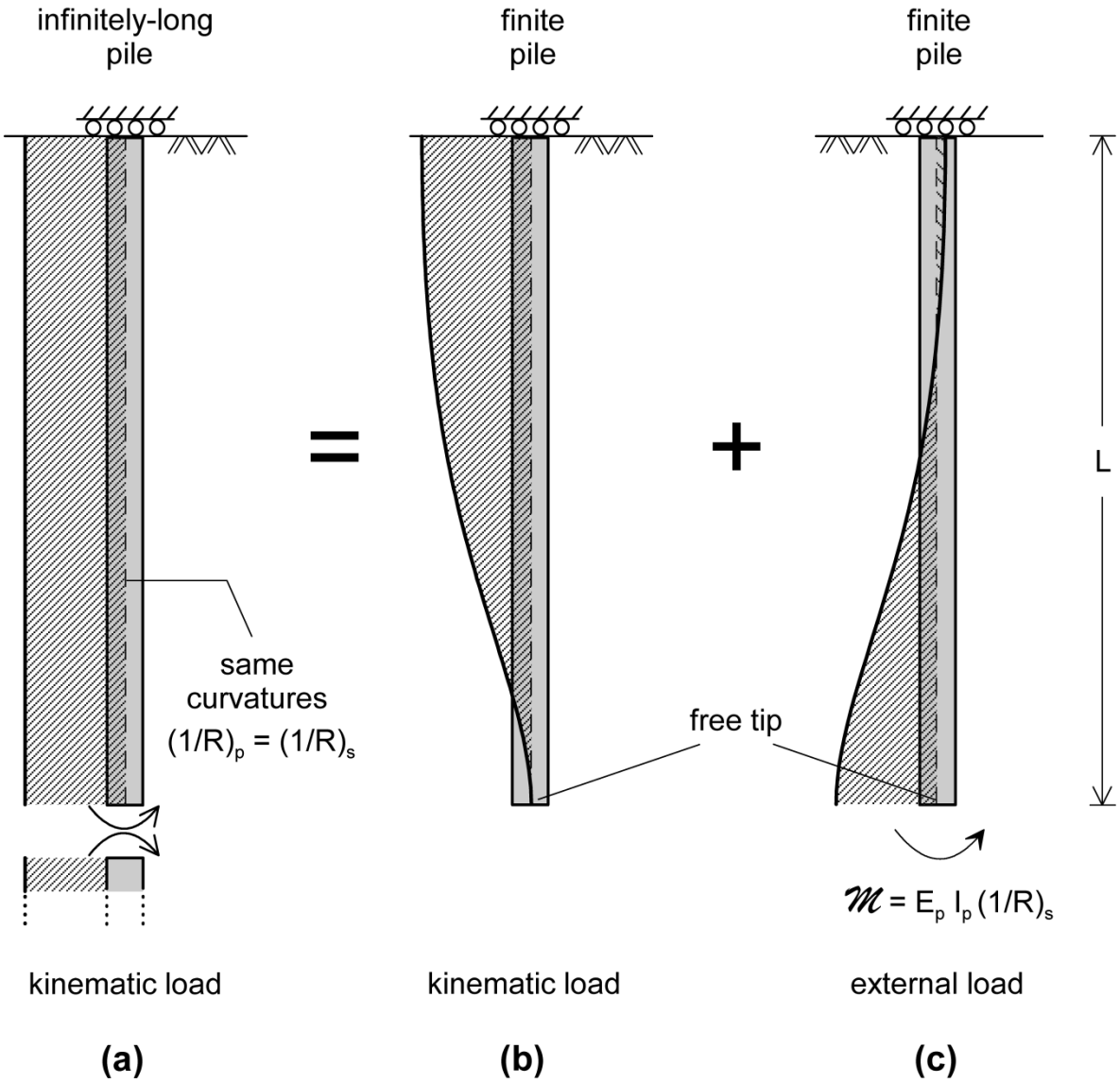

Fig. 6. Kinematic bending along an infinitely-long pile as a superposition of a kinematic and an external load on two piles of finite length (Hatched areas denote bending moment).

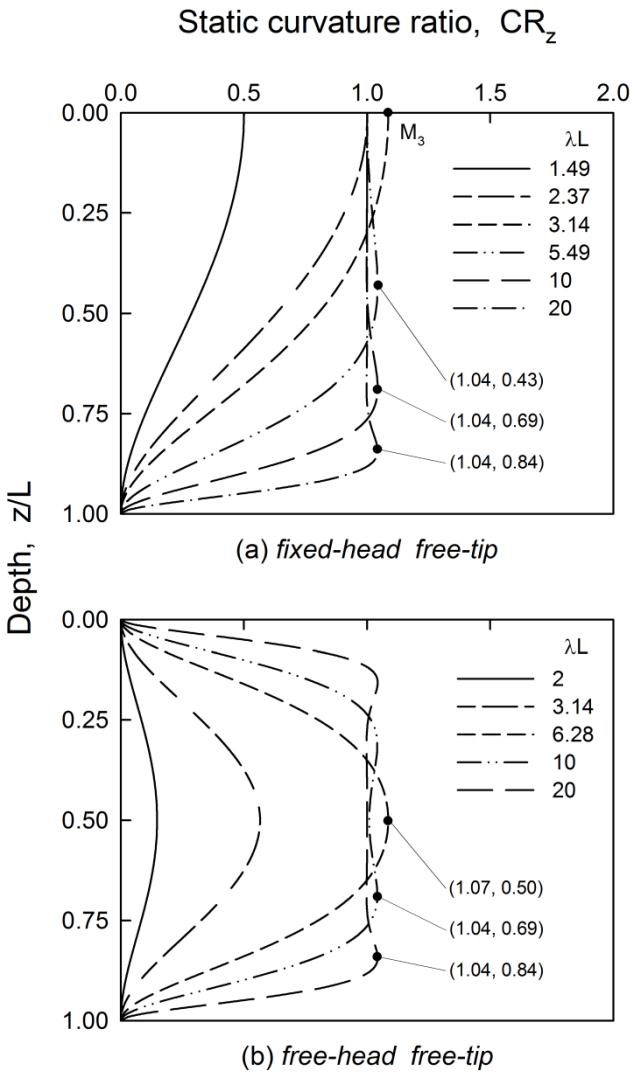

Fig. 7. Variation of static pile-soil curvature ratio with depth for free-tip piles, for different geometric and material configurations.

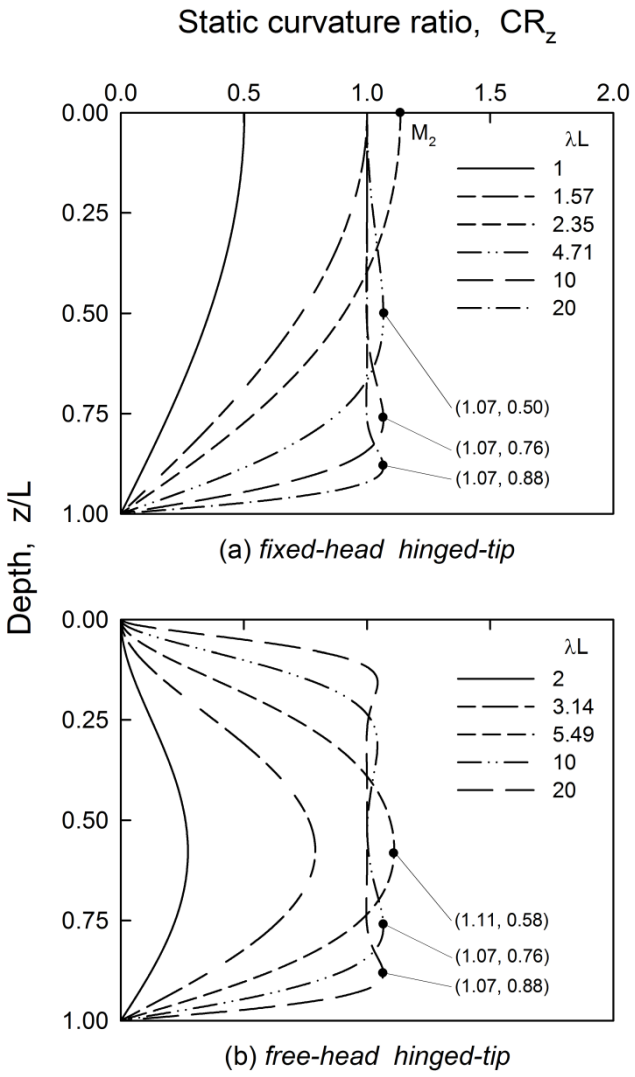

Fig. 8. Variation of static pile-soil curvature ratio with depth for hinged-tip piles, for different geometric and material configurations.

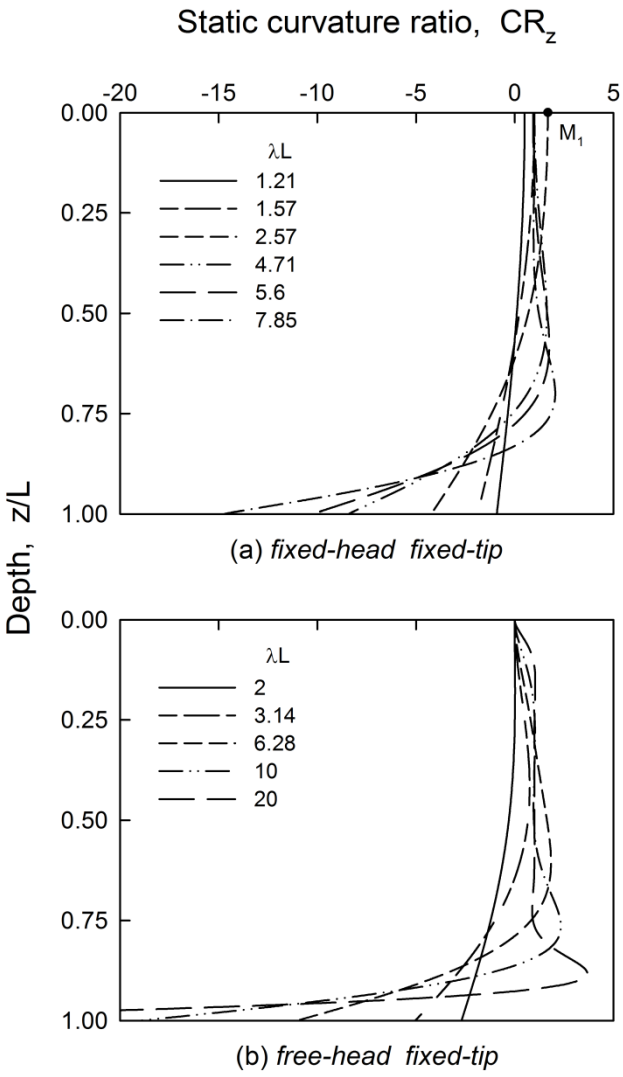

Fig. 9. Variation of static pile-soil curvature ratio with depth for fixed-tip piles, for different geometric and material configurations.

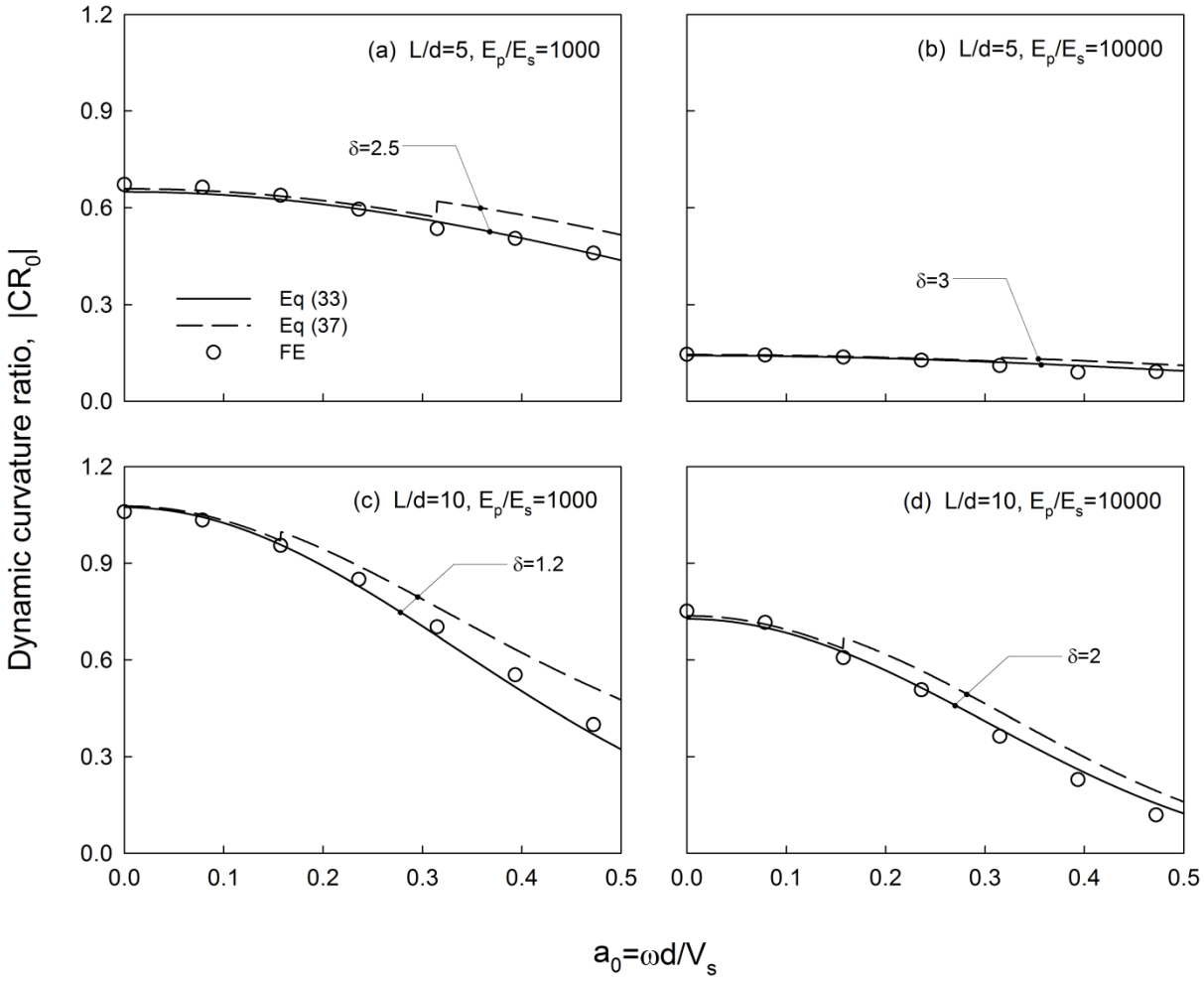

Fig. 10. Variation of dynamic pile-soil curvature ratio at pile head with frequency for fixed-head free-tip piles, for different geometric and material configurations: comparisons of rigorous elastodynamic FE results with Winkler solutions obtained using the optimum static δ value in Fig. 3. β_s=0.10

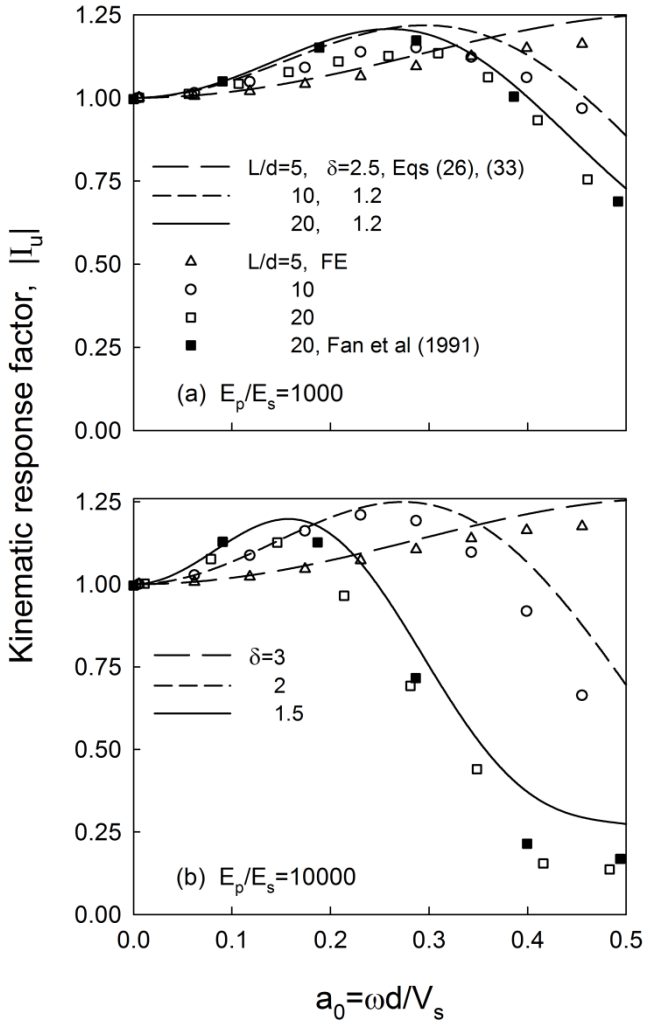

Fig. 11. Variation of kinematic response factor I_u for free-head free-tip piles: comparisons of rigorous elastodynamic FE results with Winkler solutions obtained using the optimum static δ value in Fig. 3. β_s=0.05

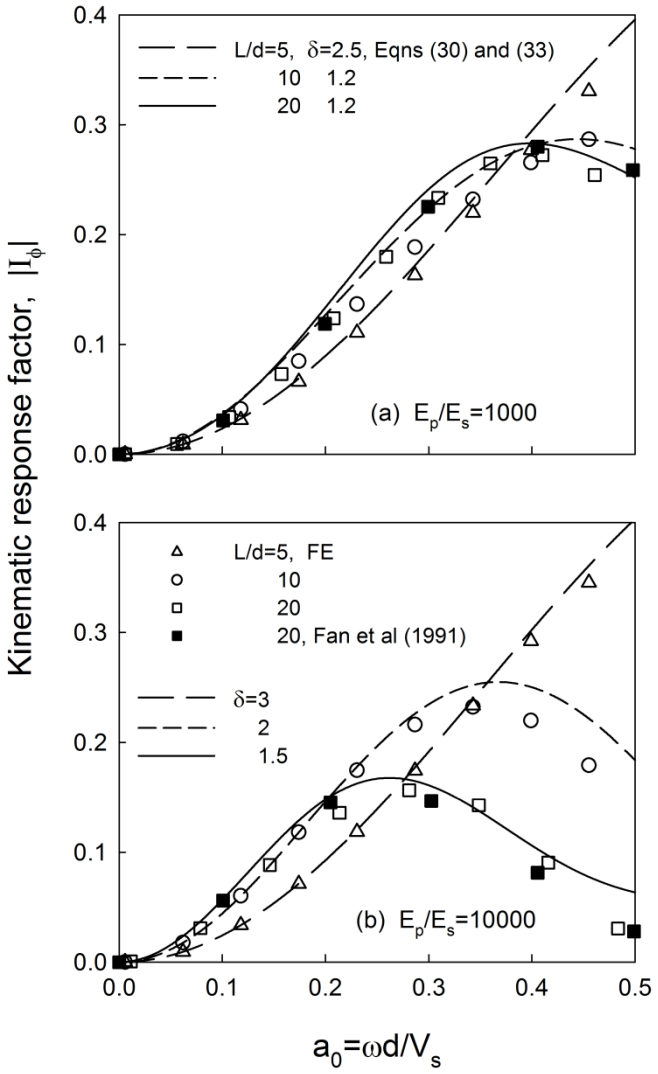

Fig. 12. Variation of kinematic response factor I_{φ} for free-head free-tip piles: comparisons of rigorous elastodynamic FE results with Winkler solutions obtained using the optimum static δ value in Fig. 3. β_s=0.05

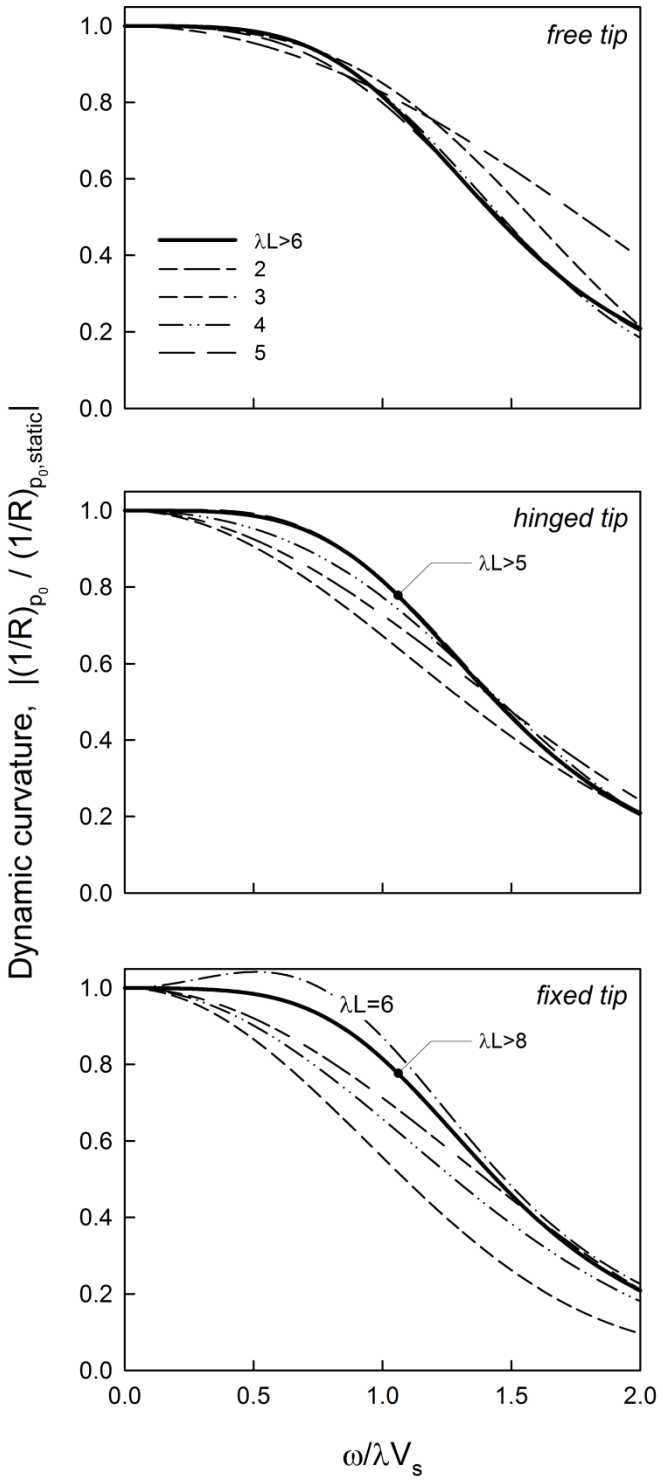

Fig. 13. Variation of dynamic pile curvature ratio at pile head with frequency for fixed-head piles under different tip conditions.

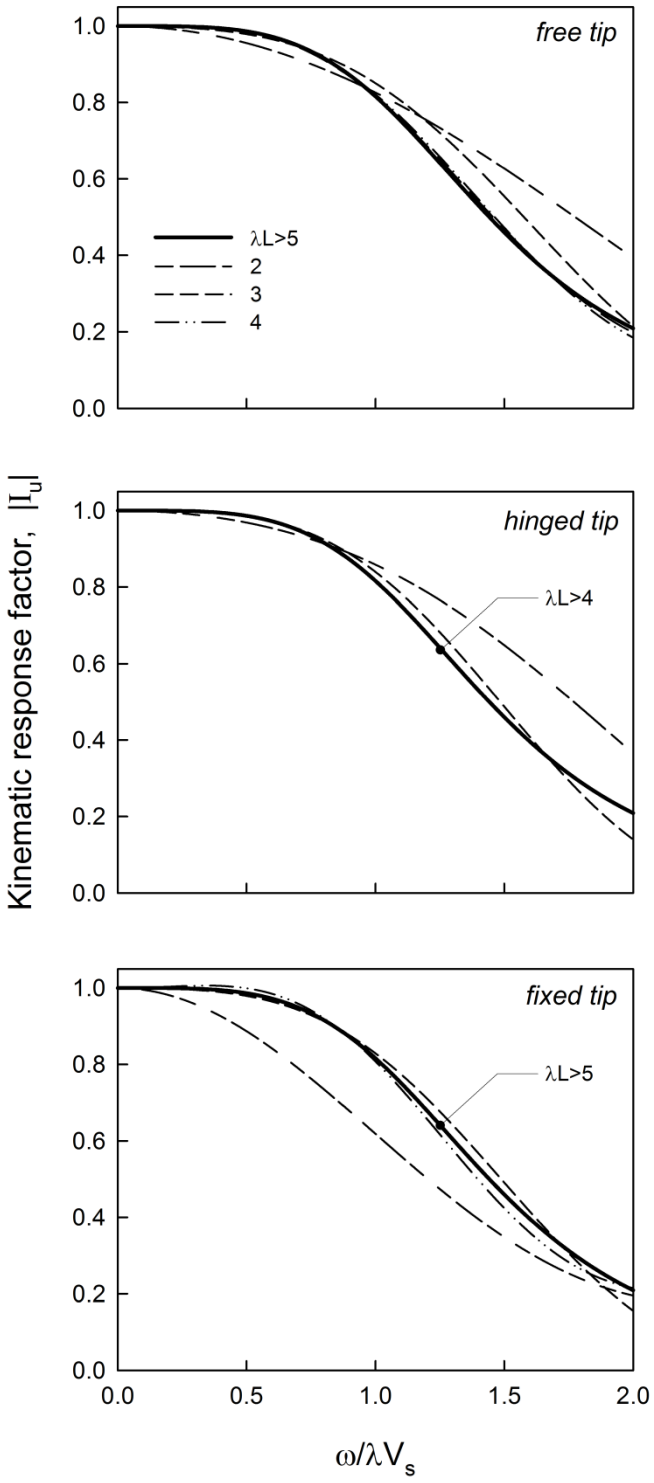

Fig. 14. Variation of kinematic response factor I_u with frequency for fixed-head piles under different tip conditions.

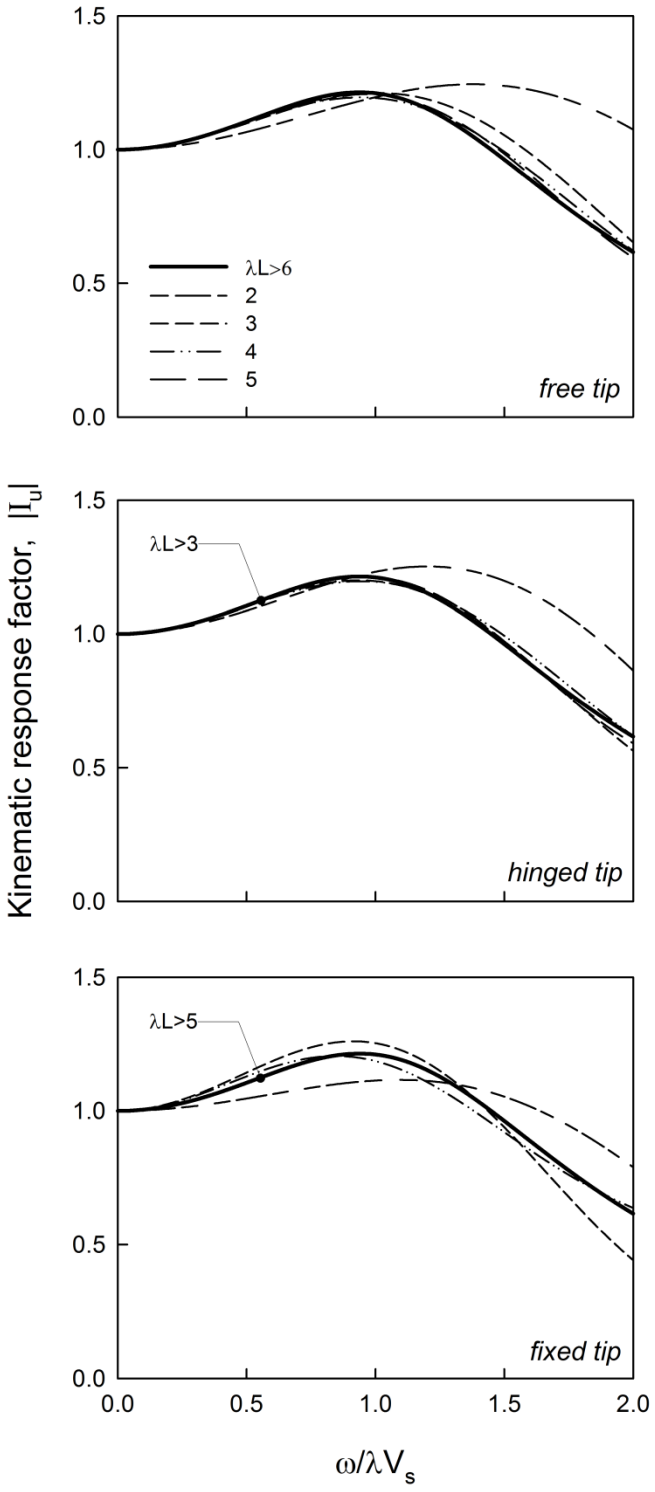

Fig. 15. Variation of kinematic response factor I_u with frequency for free-head piles under different tip conditions.

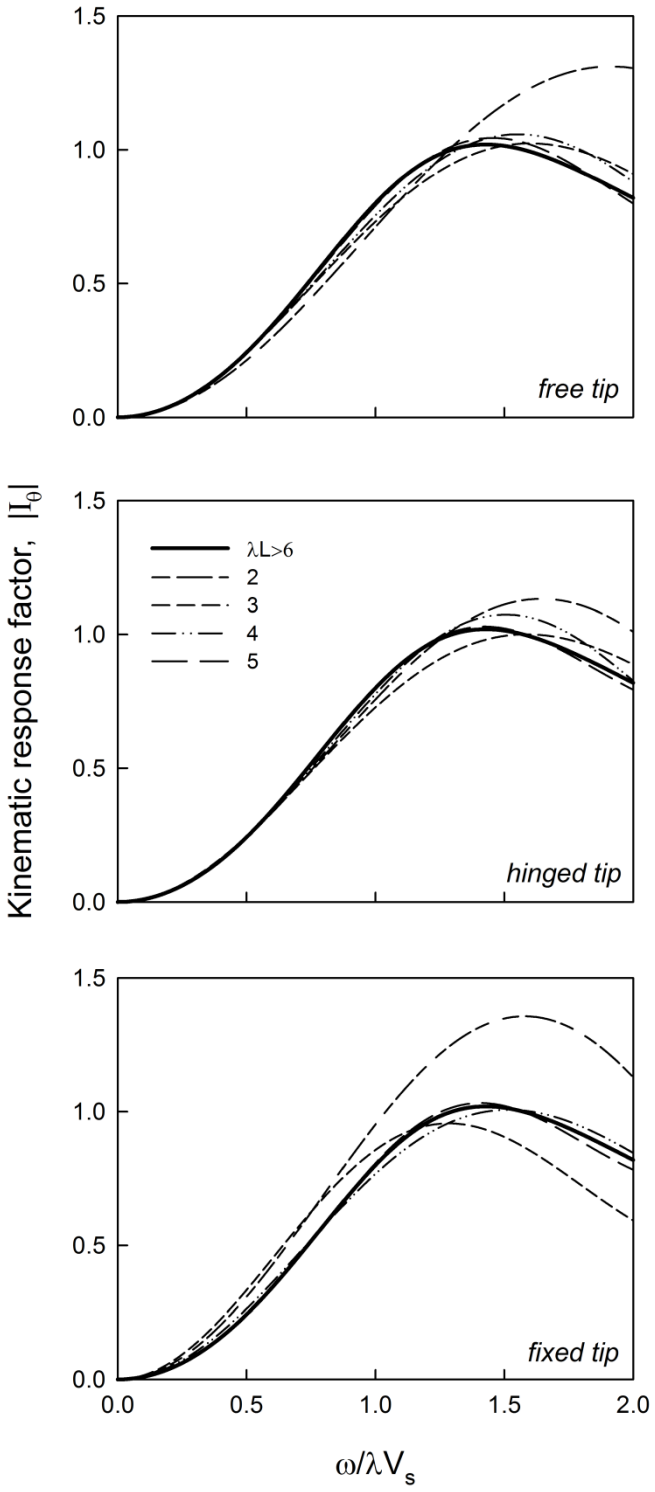

Fig. 16. Variation of kinematic response factor I_θ with frequency for free-head piles under different tip conditions.